ADVANCED ELECTRONIC MATERIALS
www.advelectronicmat.de

Hierarchical Tin Oxide Nanostructures for Dye-Sensitized Solar Cell Application

*Marwa Abd-Ellah, Samad Bazargan, Joseph P. Thomas, Md Anisur Rahman, Saurabh Srivastava, Xiongyao Wang, Nina F. Heinig, and Kam Tong Leung**

Nanoscale material manipulation is the key to increasing solar light harvesting and photon-to-electron conversion efficiency (PCE) for an organic–inorganic photovoltaic system. Many SnO_2 1D nanostructures, including nanowires and nanobelts, have been employed because of their potential of enhancing the charge collection properties of DSSCs by eliminating losses caused by grain boundary scattering of carriers in nanoparticle-based DSSCs. Here, a new approach to growing hierarchical 1D SnO_2 nanostructured layer by catalyst-assisted pulsed laser deposition after introducing NiO into the SnO_2 target is reported, and a plausible growth mechanism to describe the observed hierarchical nanostructures is presented. A remarkable improvement in the solar cell performance, including open circuit voltage, short circuit current density, fill factor, and PCE, by simple surface modification of the hierarchical SnO_2 nanostructured photoanode is further demonstrated. Surface passivation is achieved on the as-deposited hierarchical SnO_2 nanostructures by dip coating with an MgO passivation layer of appropriately optimized thickness. Such an insulating layer is found to effectively reduce the recombination process caused by the higher electron mobility of SnO_2 photoanode nanostructures. Compared with a pristine SnO_2 nanobelt photoanode, a tenfold enhancement in their PCE (to 4.14%) has been observed for MgO-passivated hierarchical SnO_2 nanostructures.

1. Introduction

Dye-sensitized solar cells (DSSCs) are promising devices for conversion of solar energy to electricity since the groundbreaking work of Gratzel.[1] During the last two decades, a massive amount of work has been done on TiO_2-based DSSCs, the photon-to-electron conversion efficiency (PCE) of which has been improved significantly, reaching as high as 10%. Recently, the use of alternative transparent conductive oxides, such as ZnO and SnO_2, has been reported for DSSC applications due to their excellent optical transparency, wide direct bandgap, high electron mobility, and large electron diffusion coefficient.[2,3] However, earlier studies have shown that ZnO could suffer from its lower chemical stability and dye loading capacity, which makes it less attractive as a photoanode in DSSC applications.[4] In contrast, SnO_2 has lower UV degradation characteristic with a bandgap of 3.8 eV and generally better stability. One major challenge of SnO_2 is the faster recombination rate due to higher electron transport dynamics and low open circuit voltage (≈400 mV), which limits the overall PCE.[5,6] Consequently, further modifications have been introduced on the surface of SnO_2 nanowires by decorating with TiO_2 nanoparticles[6] or coating with a compact thin film of MgO as a passivation layer. The latter has been shown to reduce the loss resulting from the recombination of electrons injected to SnO_2 with acceptors in the electrolyte.[5–9] Furthermore, in order to reduce the charge carrier recombination rate, which is partly due to the charge-hopping transport mechanism in classical nanoparticle films, quasi 1D nanostructures with direct pathways have been employed to improve the charge collection efficiency.[10] However, those structures generally have a lower surface area, which results in lower dye loading efficiency. Therefore, many hierarchical nanostructures have been introduced instead, in order to increase the surface area, which should improve the charge collection efficiencies and the overall performance of the DSSC.[11–13] In the present work, we employ the pulsed laser deposition (PLD) technique to produce novel SnO_2 hierarchical nanostructures by introducing NiO to create new nucleation sites. This process induces growth of nanobelt side branches off the nanobelt main trunk to produce a highly branched structure with a much higher surface area. In addition, we achieve further tuning of the open circuit voltage (V_{OC}) by simple surface passivation treatment of these hierarchical SnO_2 nanostructures with uniform coating of an MgO layer, with thickness appropriately optimized. A tenfold enhancement in the PCE of the hierarchical SnO_2 nanostructured sample with MgO passivation (to 4.14%) relative to that of a pristine SnO_2 nanobelt sample is observed.

M. Abd-Ellah, S. Bazargan, J. P. Thomas,
Md A. Rahman, S. Srivastava, X. Wang, N. F. Heinig,
K. T. Leung
WATLab and Department of Chemistry
University of Waterloo
200 University Avenue West
Waterloo, Ontario N2L3G1, Canada
E-mail: tong@uwaterloo.ca

DOI: 10.1002/aelm.201500032

ADVANCED ELECTRONIC MATERIALS
www.advelectronicmat.de

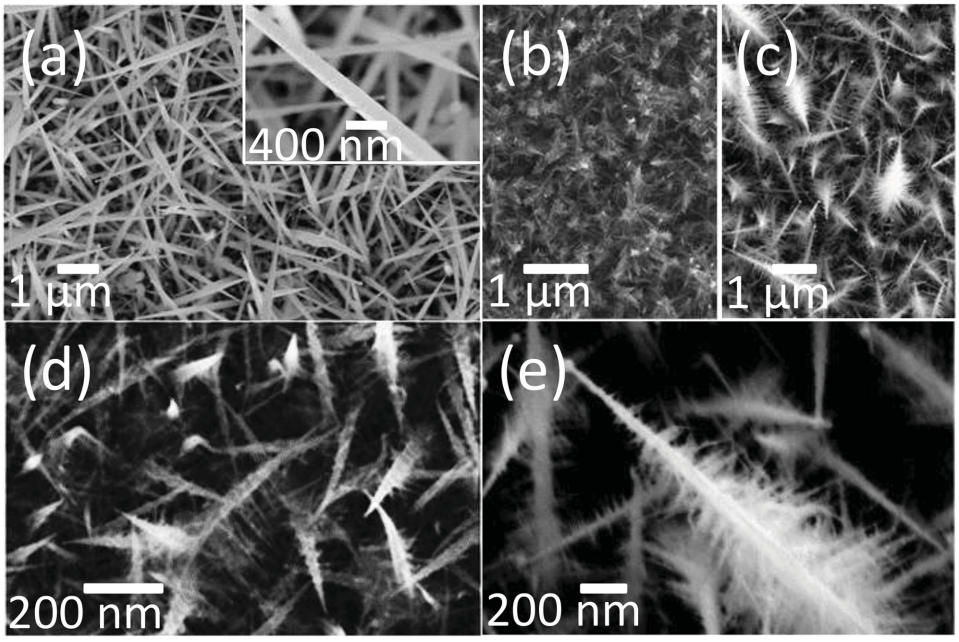

Figure 1. SEM images of a) pristine SnO_2 nanobelts with inset at a higher magnification, b,d) NiO–SnO_2 hierarchical nanostructures, and c,e) MgO/NiO–SnO_2 hierarchical nanostructures (with an MgO passivation layer of an optimized thickness). All the nanostructures were PLD-grown on ITO-glass substrates predecorated with gold nanoislands at 500 °C in 400 mTorr of Ar for 90 min.

2. Results and Discussion

2.1. Growth Mechanism of Hierarchical SnO_2 Nanostructures

The SEM images in **Figure 1** show the different morphologies of pristine SnO_2 nanobelts PLD-grown by using an SnO_2 target, highly branched hierarchical nanostructures grown by using an NiO–SnO_2 target, without and with passivation by MgO (the latter is denoted as MgO/NiO–SnO_2). The pristine SnO_2 tapered nanobelts, with typical lengths of 30–70 μm and widths of 5–30 nm, as grown on an ITO substrate predecorated with Au nanoislands are found to be in random orientation (Figure 1a). A sharp tip with a gold nanoparticle at the top of a nanobelt is observed. Interestingly, the structure changes completely into a hierarchical nanostructure (Figure 1b,d) when using an NiO-mixed SnO_2 target. The resulting side branches are 50–100 nm long, with an Au nanoparticle at the top of each of the tapered nanobelts. The roughened surface of the main nanobelt trunk and the addition of the side branches found for the NiO–SnO_2 nanostructure (Figure 1d) are clearly quite different from the pristine SnO_2 nanobelt sample (Figure 1a). We do not observe any further branching of the nanobelt side branches. The absence of any further branching confirms the important role of NiO, since the side branches need to achieve a certain diameter in order for the concentration of surface NiO to sufficiently impact the gold mobility as discussed in detail below.

These NiO–SnO_2 hierarchical nanostructures have considerably larger surface area than the pristine SnO_2 nanobelts, and therefore they are an excellent candidate for use as a photoanode for DSSC application. To further improve performance, we perform MgO passivation of these highly branched Ni-SnO_2 nanostructures, which results in a fine uniform coating of a thin MgO layer (Figure 1c,e) with much smoother surface. Evidently, the ultrasmall features are found to be preserved after the surface treatment, which suggests the viability of fabricating hybrid devices based on these hierarchical nanostructures by using this process.

The corresponding GIXRD results (Supporting Information, Figure S1) show very similar results for the PLD-grown SnO_2 nanobelts and NiO–SnO_2 hierarchical nanostructures, both with a preferred growth direction of (110), while the hierarchical nanostructures are found to have a higher (100) intensity for the $Au_{17}Sn_3$ alloy feature. Furthermore, no shift in the X-ray peak position from the literature values for SnO_2 (00-041-1445) is observed, with the full width at half maximum also showing little or no broadening, consistent with a pure material. This finding confirms the absence of any doping effect of NiO on the SnO_2 crystal structure due to their low solubility, in accord with the results of Castro et al.[14] Lowering the NiO concentration in the NiO–SnO_2 target has led to larger and longer primary SnO_2 nanobelts before the formation of side branches, while increasing the NiO concentration has given rise to smaller primary SnO_2 nanobelts and potentially more side branches.

The crystal structures of the as-grown hierarchical nanostructures have also been examined by TEM. The low-resolution TEM image (**Figure 2**a) shows a typical PLD-grown NiO–SnO_2 hierarchical nanostructure, in which the tapered nanobelts are capped with gold nanoparticles. The corresponding high-resolution TEM images for the nanoparticle (Figure 2b) and side branch regions (Figure 2c) reveal respective fringe spacings of 0.23 and 0.33 nm, which correspond to the interplanar spacings along the Au[111] (Figure 2b) and SnO_2[110] directions (Figure 2c), respectively. Fourier transform patterns

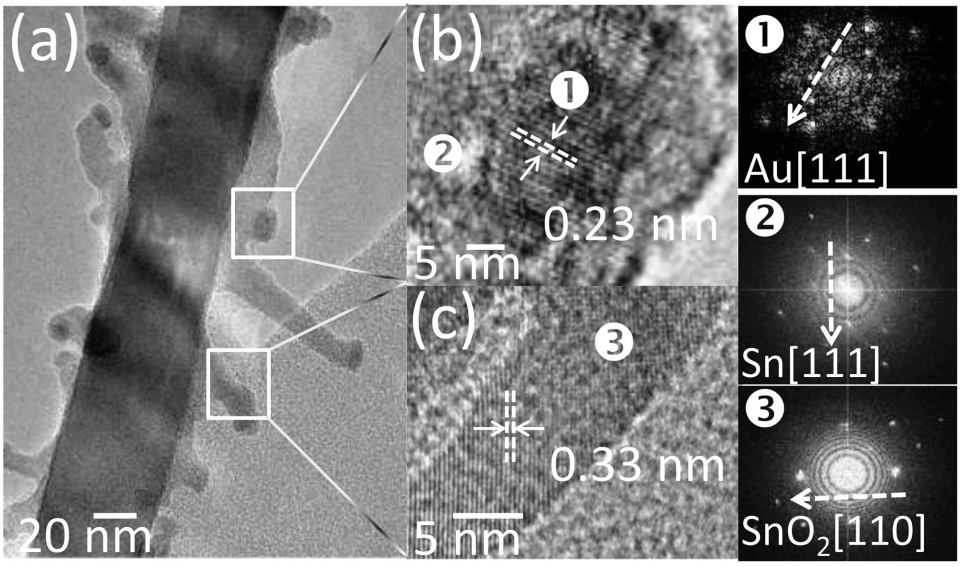

Figure 2. a) Low-resolution and b,c) high-resolution TEM images for a typical NiO–SnO_2 hierarchical nanostructure with fringe spacings corresponding to different crystalline planes for region 1: gold nanoparticles, region 2: metallic Sn, and region 3: SnO_2 side branch, with different respective growth orientations. Respective Fourier transform patterns for selected regions 1, 2, and 3 are shown on the far right.

(Figure 2, far right panels) are also obtained for the catalyst region (Region 1), outer region of the catalyst (Region 2), and the nanobelt region (Region 3). These patterns are found to be consistent with the identification of the respective regions to Au, metallic Sn, and SnO_2, respectively. The existence of a gold–tin alloy was observed in our earlier work[15] and our results are in accord with previous studies on the catalytic role of metallic Sn nanoparticles in the growth of other semiconductors,[16,17] and the self-catalytic property for the growth of SnO_2 nanowires and nanobelts.[18,19]

In **Figure 3**, we show a schematic diagram of our proposed mechanism for the growth of these hierarchical structures. In our model, Au nanoisland formation on an ITO-glass substrate (Stage a) provides the catalysts for PLD-growth of SnO_2 nanobelts following the vapor–liquid–solid growth mechanism (Stage b). This process is catalyzed with the gold nanoparticle at the top of the nanobelt. As soon as there is a sufficiently large SnO_2 nanobelt surface, the NiO nanoclusters are adsorbed on the surface due to the low solubility of NiO in SnO_2.[15] These NiO nanoclusters on the SnO_2 nanobelt surface would lower the mobility of gold catalysts on the surface, which are relatively mobile at deposition temperature of 500 °C. The lower mobility of gold catalysts leads to the formation of smaller gold nanoparticles on the edges of the nanobelt (Stage c). These NiO+Au nanoclusters could serve as possible reaction sites that promote the reduction of Sn^{2+}/Sn^{4+} to metallic Sn on the nanobelt edge (Stage d). The Sn atoms interacting with the mobile gold atoms form the Sn–Au alloy nucleation sites that catalyze growth of SnO_2 side branches off the trunk of the nanobelt, following the vapor–liquid–solid growth mechanism (Stage e) with higher

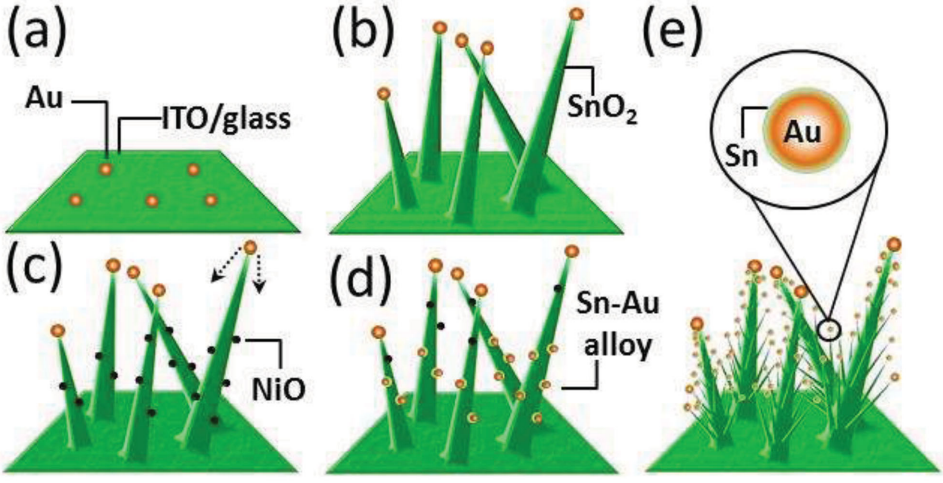

Figure 3. Schematic diagram of our proposed growth mechanism for a typical NiO–SnO_2 hierarchical nanostructure grown by catalyst-assisted PLD using an SnO_2 target mixed with NiO.

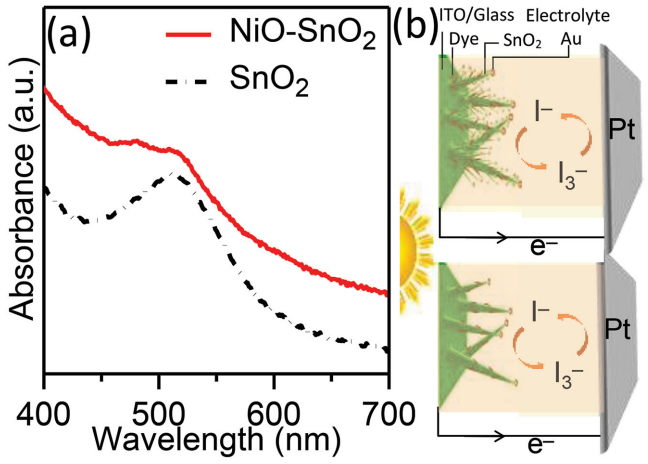

Figure 4. a) UV–vis absorption spectra for pristine SnO_2 nanobelts and NiO–SnO_2 nanostructures, depicting a higher dye loading for the NiO–SnO_2 hierarchical nanostructures than the pristine SnO_2 nanobelts due to the increase in surface area. b) Schematic diagrams of DSSC device structures employing pristine SnO_2 nanobelts (top) and NiO–SnO_2 hierarchical nanostructures (bottom) as the photoanode materials.

magnification of the gold particles surrounded with metallic Sn shell as will be confirmed later. This process is self-limited by the finite amount of NiO (5%) present in the target, creating the hierarchical nanostructures without any secondary side branch generation. Consistent with our XRD results, no doping effect of NiO is detected as shown in Figure 2c, as no change in the SnO_2 lattice spacing is observed. Growth of the hierarchical structures should depend sensitively on the NiO concentration in the SnO_2 target, because a critical surface concentration of NiO is required to lower the gold mobility. The effect of NiO can be inferred by the presence of a thin layer of metallic Sn coating the gold nanoparticles located at the tips of the side branches and of the main trunks of SnO_2 nanobelts. The presence of the metallic Sn coating is supported by the Fourier transform patterns of region 2 in Figure 2.

2.2. SnO_2 Nanostructures as Photoanodes for DSSC Application

The increase in the surface area of the NiO–SnO_2 hierarchical nanostructures can be estimated by measuring the enhancement of dye adsorption. Prior to our dye loading measurements, a calibration curve of the Z907 dye at different concentrations was constructed (Supporting Information, Figure S2). The UV–vis absorption spectra were collected after incubating both the pristine SnO_2 nanobelts and hierarchical NiO–SnO_2 nanostructures in the dye overnight. This was followed by desorption of the adsorbed dye from the nanostructures using 10×10^{-3} M KOH at pH 13 and evaluation of the concentrations of the desorbed dye for both samples from their UV–vis spectra. **Figure 4**a shows a higher dye absorbance for the NiO–SnO_2 hierarchical nanostructures giving a dye concentration of 8.6×10^{-6} M, in comparison to that of pristine SnO_2 nanobelts with a concentration of 7.7×10^{-6} M, all evaluated at wavelength of 522 nm. This result confirms the larger surface area of the as-prepared NiO–SnO_2 hierarchical nanostructures.

In Figure 4b, we show the schematic diagrams of the DSSCs that we fabricated using the pristine SnO_2 nanobelts and NiO–SnO_2 hierarchical nanostructures as the photoanodes. The increase in the adsorption areas provided by NiO–SnO_2 hierarchical nanostructures results in greater adsorption of the dye, which in turn increases the solar cell performance, as discussed below.

Figure 5a shows the current density versus voltage curves obtained over an active area of 0.1 cm^2 for different DSSCs employing as active photoanode materials: pristine SnO_2 (Cell A), hierarchical NiO–SnO_2 (Cell B), and hierarchical NiO–SnO_2 nanostructures passivated with an MgO layer, designated as MgO/NiO–SnO_2 (Cell C). For Cell C, we varied the thickness of the MgO passivation layer by incubating the sample in different concentrations of hot ethanolic $Mg(CH_3COO)_2$: (C20) 20×10^{-3} M, (C60) 60×10^{-3} M, and (C120) 120×10^{-3} M, all followed by annealing in air at 500 °C for 90 min. Their solar cell performances, along with their cell structures, are summarized in Figure 5 and **Table 1**. Although great enhancement by nearly an order of magnitude is observed in the short circuit current density (J_{SC} = 18.57 mA cm^{-2}) for Cell B due to a higher dye loading arising from a larger surface area of the hierarchical NiO–SnO_2 nanostructures, both open circuit voltage (V_{OC} = 0.414 V) and fill factor (FF = 48%) for Cell B are slightly lower than the respective values for Cell A (with V_{OC} = 0.463 V, FF = 55%, and J_{SC} = 1.87 mA cm^{-2}). This finding confirms a more pronounced effect that the higher mobility in SnO_2 leads to a higher probability of recombination of electrons injected to SnO_2 with acceptors in the electrolyte.[9] In order to reduce the recombination loss, we coated an insulating layer of MgO with different thicknesses using hot ethanolic $Mg(CH_3COO)_2$ solutions of different concentrations, as shown in the schematic band diagram of the constructed cell (Supporting Information, Figure S3). For a thicker MgO film coating obtained with a higher concentration for Cell C120, up to 0.3 V improvement in V_{OC} to 0.710 V and 15.9% increase in FF to 71% with respect to Cell B are obtained. However, this is accompanied by a drastically lower J_{SC} of 1.83 mA cm^{-2}, indicating sharp retardation in charge carrier diffusion likely caused by a thicker passivation layer. Further investigation was conducted to optimize the passivation layer thickness by studying the effect of different concentrations of $Mg(CH_3COO)_2$ on both J_{SC} and V_{OC}, as well as the overall PCE, as shown in Figure 5. Evidently, an increase of 0.138 V in V_{OC} for C20, followed by higher values of 0.188 V for C60 and 0.296 V for C120, all with respect to V_{OC} for Cell B, is observed (Figure 5b). At the same time, sharp increase in J_{SC} is found for Cell B (compared with Cell A), followed by a generally reducing trend from B to C20, C60, and C120 (Figure 5c). An optimum concentration of 20×10^{-3} M was obtained for Cell C20, with J_{SC}, V_{OC}, and FF of 13.34 mA cm^{-2}, 0.547 V, and 52%, respectively, leading to a notable increase in PCE (to 4.14%) from the PCEs of Cell A (0.48%) and Cell B (3.69%). However, this increase in PCE is at the expense of a smaller J_{SC}, which can be explained by the blue shift in the photocurrent of insulating coating.[20] Recent studies have employed SnO_2 films and nanostructures, mostly prepared by hydrothermal methods, as the photoanode material for DSSC applications, the PCE of which was found to increase by up to 7% after passivation process.[7,8,10,20,21] To date, even fewer studies have used SnO_2

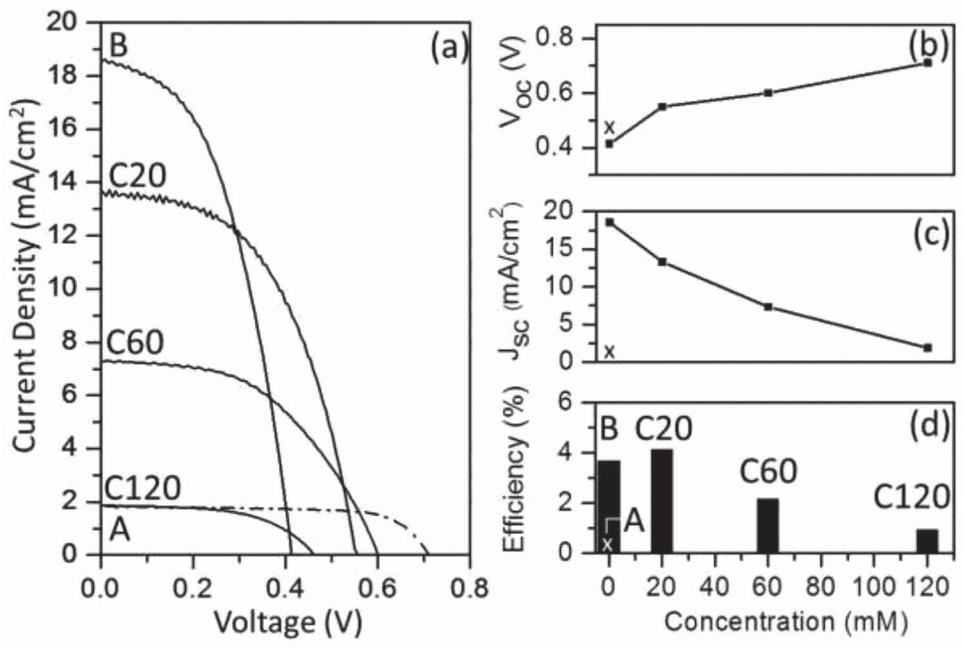

Figure 5. a) Current density versus voltage profiles, b) open circuit voltage, c) short circuit current density, and d) photoconversion efficiency of DSSCs with different photoanode materials: (Cell A) pristine SnO_2 nanobelts (marked by cross), (Cell B) NiO–SnO_2 hierarchical nanostructures, and (Cell C20, C60, C120) NiO–SnO_2 hierarchical nanostructures passivated with MgO layers of different thicknesses.

nanomaterials grown by vapor deposition methods for DSSC applications. Gubbala et al. employed ALD-grown SnO_2 nanowires as a photoanode with an excellent open circuit voltage of 0.560 V and an overall PCE of 2.1%. Furthermore, an enhancement in their performance of 4.1% was obtained by coating the highly interconnected nanowires with TiO_2 nanoparticles.[6] In the present work, a remarkable enhancement in PCE, i.e., over seven times increase, for Cell B is observed when compared with pristine SnO_2 nanobelts (Cell A). While fine tuning of the thickness of the MgO passivation layer appears to improve the PCE by only 12% for Cell C20 from that without any passivation layer (Cell B), the improvement in V_{OC} by 33% for Cell C20 (and 71% for Cell 120) with respect to that for Cell B is significant. Future work will focus on further optimization of the deposition parameters to obtain better length to width aspect ratio for the as-grown SnO_2 nanostructure for electronic applications. In addition, in situ decoration with Au or Ag nanoclusters in the hierarchical SnO_2 nanostructures during PLD growth may offer additional improvement on their PCEs through plasmonic effects.

Table 1. Solar cell performance of DSSCs with different photoanode materials: (Cell A) pristine SnO_2 nanobelts, (Cell B) NiO–SnO_2 hierarchical nanostructures, and (Cell C20, C60, C120) MgO/NiO–SnO_2 hierarchical nanostructures passivated with MgO of different thicknesses.

Cell structure[a)]		V_{oc} [V]	J_{sc} [mA cm^{-2}]	FF [%]	PCE [%]
A	SnO_2	0.463	1.87	55	0.48
B	NiO–SnO_2	0.414	18.57	48	3.69
C20	MgO/NiO–SnO_2	0.552	13.34	52	4.14
C60	MgO/NiO–SnO_2	0.602	7.30	49	2.17
C120	MgO/NiO–SnO_2	0.710	1.83	71	0.93

[a)]Cells C20, C60, and C120 were prepared with MgO passivation layers of different thicknesses obtained by soaking in, respectively, 20, 60, and 120 × 10^{-3} M of hot ethanolic Mg acetate solution at 70 °C for 1 min, followed by annealing in air at 500 °C for 90 min.

3. Conclusion

Highly branched NiO–SnO_2 hierarchical nanostructures, consisting of tapered nanobelt main trunk and nanobelt side branches with greatly increased surface area, were obtained by using an NiO-mixed SnO_2 target for catalyst-assisted PLD. We propose a plausible growth model involving NiO nanoclusters as the initiators for reducing Sn ions to metallic Sn, which then mixes with the highly mobile Au atoms (coming from the Au nanocatalyst at the tip of the nanobelt) forming Sn–Au alloy nanoclusters on the nanobelt surface. These Sn–Au alloy nanoclusters provide the nucleation sites for growth of SnO_2 side branches. Furthermore, both pristine SnO_2 nanobelts and NiO–SnO_2 hierarchical nanostructures were employed as photoanode materials in DSSCs. When compared to SnO_2 pristine nanobelts (Cell A), an excellent enhancement in J_{SC} is observed for NiO–SnO_2 hierarchical nanostructures (Cell B) due to their higher dye loading as a result of their larger surface area and better charge collection property. Furthermore, hot ethanolic $Mg(CH_3COO)_2$ solutions of different concentrations have been used to optimize coating of the as-prepared NiO–SnO_2 hierarchical nanostructures with an MgO passivation layer of appropriate thickness. This passivation step is found to be successful in reducing the large contribution of

recombination of electrons injected to SnO_2 with acceptors in the electrolyte due to the much higher electron transport dynamics of SnO_2 photoanode. With an optimized thickness for the MgO passivation layer to reduce the expected recombination loss, a nearly tenfold enhancement in the PCE to 4.14% has been achieved for MgO-passivated NiO–SnO_2 hierarchical nanostructures (Cell C20) when compared to pristine SnO_2 nanobelts (Cell A). The present work therefore illustrates the importance of increasing surface area and enhancing the charge carrier collection by developing a new approach of synthesizing hierarchical nanostructures. In addition, we succeeded in improving the open circuit voltage by minimizing recombination loss using MgO passivation with appropriately optimized layer thickness for building high efficiency dye-sensitized solar cells.

4. Experimental Section

SnO_2 nanostructures were prepared in a PLD system with an excimer laser source (248 nm) operating with a fluence of 350 mJ/pulse and a repetition rate of 10 Hz. A detailed description of the catalyst-assisted PLD system used for depositing SnO_2 nanobelts has been given elsewhere.[12] Indium tin oxide (ITO) coated glass substrates were sonicated in acetone and then in isopropanol, each for 10 min, followed by thoroughly rinsing with Millipore water before use. Following earlier work,[22] gold nanoislands were created on these substrates by postannealing a thin (<10 nm), sputter-coated layer of gold at 400–700 °C for 1 h.

Deposition targets, composed of pure SnO_2 and of SnO_2 mixed with 5 wt% NiO, were prepared by mixing and grinding appropriate amounts of respective powders in a mortar and pestle for 20 min, followed by pressing the powders under 20 MPa and sintering them for 24 h at 900 °C. Laser ablation was then performed at a substrate temperature of 500 °C in 400 mTorr of Ar for 90 min, using the respective targets of pristine SnO_2 and of NiO-mixed SnO_2 (designated here as NiO–SnO_2). The morphologies of the resulting SnO_2 nanostructured films were studied by using field-emission scanning electron microscopy (SEM) in a Zeiss Ultra Plus microscope. The crystal structures were characterized by glancing incidence X-ray diffraction (GIXRD) using a PANalytical X'Pert Pro MRD diffractometer, configured with a mirror incident beam optics and 0.27° parallel plate collimator on the diffracted beam optics, at an incidence angle of 0.6°. Bright-field low-resolution and high-resolution transmission electron microscopy (TEM) studies were performed by using a Zeiss Libra 200 MC microscope on hierarchical nanostructures scraped off from the substrate and transferred onto a lacey carbon TEM grid.

The surface areas of the samples were estimated by desorption experiments. Commercial dye solutions (Z907, Solarnix) with different concentrations were prepared and their UV–vis absorption spectra were collected. Using the Beer–Lambert law, a calibration curve was constructed based on the absorbance of different dye concentrations at different wavelengths (λ). The molar absorption coefficient of the dye was also calculated to be 4.205 m^2/mol at a fixed λ_{max} = 522 nm. Both dye-loaded pristine SnO_2 and NiO–SnO_2 samples were each placed into a 10×10^{-3} M solution of KOH (pH 13) to desorb the dye. The concentrations of the desorbed dye were determined by UV–vis spectroscopy and the amount of dye loading was calculated.[23]

The as-prepared nanostructures was passivated by further surface treatment of dipping in a hot ethanolic $Mg(CH_3COO)_2$ solution of three different concentrations (20, 60, and 120×10^{-3} M) for 1 min at 70 °C. A passivated shell layer of MgO covering the nanostructures (with thickness depending on the $Mg(CH_3COO)_2$ concentration) was then generated by annealing in air at 500 °C for 90 min.[7]

In the present work, a DSSC was prepared using a standard procedure as follows. The photoanode was obtained by soaking the as-prepared SnO_2 or NiO–SnO_2 nanostructures (supported on an ITO-glass substrate) in a 0.3×10^{-3} M solution of the Z907 dye for 72 h. A Pt thin film (200 nm thick) sputter-deposited on the ITO-glass substrate was used as the counter electrode. A redox couple electrolyte ($3I^-/I_3^-$) was then sandwiched between the photoanode and the counter electrode. The corresponding electrical parameters were characterized by using a solar cell current–voltage characterization system (PV Measurements IV5) equipped with a class ABA solar simulator and an Air Mass 1.5 global spectral filter. Prior to the current–voltage measurement, the system was calibrated using an Si reference cell (PVM782 with a BK7 window).

Supporting Information

Supporting Information is available from the Wiley Online Library or from the author.

Acknowledgement

This work was supported by the Natural Sciences and Engineering Research Council of Canada.

Received: January 18, 2015
Revised: June 3, 2015
Published online: July 8, 2015

[1] B. O' Regan, M. Gratzel, *Nature* **1991**, *353*, 737.
[2] S. H. Ko, D. Lee, H. W. Kang, K. H. Nam, J. Y. Yeo, S. J. Hong, C. P. Grigoropoulos, H. J. Sung, *Nano Lett.* **2011**, *11*, 666.
[3] H. J. Snaith, C. Ducati, *Nano Lett.* **2010**, *10*, 1259.
[4] T. P. Chou, Q. Zhang, G. Cao, *J. Phys. Chem. C* **2007**, *111*, 18804.
[5] A. N. M. Green, E. Palomares, S. A. Haque, J. M. Kroon, J. R. Durrant, *J. Phys. Chem. B* **2005**, *109*, 12525.
[6] S. Gubbala, V. Chakrapani, V. Kumar, M. K. Sunkara, *Adv. Funct. Mater.* **2008**, *18*, 2411.
[7] P. Docampo, P. Tiwana, N. Sakai, H. Miura, L. Herz, T. Murakami, H. J. Snaith, *J. Phys. Chem. C* **2012**, *116*, 22840.
[8] M. K. I. Senevirathna, P. K. D. D. P. Pitigala, E. V. A. Premalal, K. Tennakone, G. R. A. Kumara, A. Konno, *Sol. Energy Mater. Sol. Cells* **2007**, *91*, 544.
[9] A. N. M. Green, E. Palomares, S. A. Haque, J. M. Kroon, J. R. Durrant, *J. Phys. Chem. B* **2005**, *109*, 12525.
[10] S. Gubbala, H. B. Russell, H. Shah, B. Deb, J. Jasinski, H. Rypkemac, M. K. Sunkara, *Energy Environ. Sci.* **2009**, *2*, 1302.
[11] M. McCune, W. Zhang, Y. Deng, *Nano Lett.* **2012**, *12*, 3656.
[12] D. Lee, Y. Rho, F. I. Allen, A. M. Minor, S. H. Ko, C. P. Grigoropoulos, *Nanoscale* **2013**, *5*, 11147.
[13] I. Herman, J. Yeo, S. Hong, D. Lee, K. H. Nam, J. Choi, W. Hong, D. Lee, C. P. Grigoropoulos, S. H. Ko, *Nanotechnology* **2012**, *23*, 194005.
[14] R. H. R. Castro, P. Hidalgo, R. Muccillo, D. Gouveea, *Appl. Surf. Sci.* **2003**, *214*, 172.
[15] S. Bazargan, K. T. Leung, *J. Chem. Phys.* **2013**, *138*, 104704.
[16] P. X. Gao, Z. L. Wang, *J. Phys. Chem. B* **2002**, *106*, 12653.
[17] J. Y. Lao, J. Y. Huang, D. Z. Wang, Z. F. Ren, *Nano Lett.* **2003**, *3*, 235.
[18] Y. X. Chen, L. J. Campbell, W. L. Zhou, *J. Cryst. Growth* **2004**, *270*, 505.
[19] Y. C. Liang, H. Zhong, *Nanoscale Res. Lett.* **2013**, *8*, 358.
[20] A. Kay, M. Gratzel, *Chem. Mater.* **2002**, *14*, 2930.
[21] H. J. Snaith, C. Ducati, *Nano Lett.* **2010**, *10*, 1259.
[22] S. Bazargan, K. T. Leung, *J. Phys. Chem. C* **2012**, *116*, 5427.
[23] J. Han, F. Fan, C. Xu, S. Lin, M. Wei, X. Duan, Z. L. Wang, *Nanotechnology* **2010**, *21*, 405203.